Reactive and inhibiting species in the electrocatalytic oxidation of glycerol on gold. A study combining in-situ visible reflectance and ATR-SEIRAS

Laura Pérez-Martínez, Lisa Balke and Angel Cuesta*.

School of Natural and Computing Sciences, University of Aberdeen, Aberdeen AB24 3UE, Scotland, UK

*Corresponding author: angel.cuestaciscar@abdn.ac.uk

ABSTRACT

By combining cyclic voltammetry and potentiostatic current transients with measurements of the potential dependence of gold's reflectance at 520 nm, we provide unambiguous evidence that glycerol and gold oxidation compete for adsorbed OH, whereby the formation of gold oxide is retarded in the presence of glycerol and the formation of gold oxide inactivates the oxidation of glycerol. Potentiostatic current transients coupled with ATR-SEIRAS at potentials close to the onset of glycerol oxidation also suggest that the adsorption of carboxylates generated upon oxidation of glycerol leads to a progressive decrease of the electrocatalytic activity. However, both ATR-SEIRAS and experiments using a rotating-disk electrode suggest that the adsorption of these carboxylates is an equilibrium process. Therefore, using high flow rates should allow to keep the inhibition of the reaction at an acceptable level. These results are relevant for the design of fuel cells capable of generating electricity plus value-added chemicals from glycerol.

Keywords: Glycerol; fuel cell; gold; OH_{ad}; gold oxide; visible reflectance; ATR-SEIRAS

1. Introduction

An efficient use of renewable energy resources such as wind, solar and biomass is necessary to escape our reliance on non-renewable fossil fuel resources, such as petroleum, natural gas and coal, which results in emission of pollutants and global warming. Specifically, biofuels obtained from biomass are regarded as a promising alternative to fossil fuels, and using them as the fuel in a fuel cell, instead of an internal combustion energy, would make their conversion to energy more efficient [1,2].

The electrocatalysis of organic molecules like higher alcohols has long since attracted interest, largely because they have higher volume energy densities than gaseous fuels such as hydrogen and natural gas [3–6]. Glycerol is a largely available, inexpensive and inherently renewable compound, generated as a by-product from biofuel industries [1]. Total oxidation to CO_2 involves the exchange of 14 electrons and 14 protons, which, together with the need to activate two C-C bonds makes it a reaction with a complex mechanism which requires a significant overpotential [7,8]. Its partial oxidation to C2 or C3 products, however, is also appealing, because it can result in some products with higher economic value than glycerol, such as glyceric acid or glycolic acid, with applications in medicine, cosmetics and the textile industry [1,9], among others. An alternative to complete oxidation is therefore to use glycerol as a fuel in a fuel cell producing chemicals with a higher value-added at no energy cost or, in particularly favourable cases, coupled to the generation of energy, thereby obtaining a double benefit [8,10].

As with all alcohols, oxidation of glycerol is easier in alkaline media. As has been shown by Kwon et al. [11], this implies that the dissociation of the OH group is the first step and that the alkoxide alcoholate ($R\text{-}O^-$), rather than the alcohol itself, is the active species. At pHs less than two units below the alcohol's pK_a, less than 1% of the alcohol will be in the active form, and oxidation currents are very small. In acidic media, gold shows no electrocatalytic activity towards glycerol oxidation and even typically very active catalysts like Pt show very little

activity [12]. Evidence of total oxidation of glycerol to carbonate in alkaline media has been found using external reflectance IR spectroscopy on both Pt [13,14] and Au [14,15]. Detection of CO_2 as a product of the oxidation of glycerol on gold in initially alkaline solutions has also been reported using external reflectance FTIR spectroscopy [15], but this was obviously due to a reaction-induced considerable decrease of the pH in the thin electrolyte layer trapped between the electrode and the window. External reflectance FTIR has been used by other authors in an attempt to identify reaction products [7,8], although this is not the most appropriate technique for that purpose, because of the lack of control of important experimental parameters like the pH, and because of the depletion of reactants and accumulation of products in the thin electrolyte layer trapped between the electrode and the window. The huge electrolyte resistance associated to the thin layer configuration also leads to a loss of control of the actual electrode potential, particularly when large currents are flowing. Surface-enhanced infrared absorption spectroscopy in the attenuated total reflection mode (ATR-SEIRAS) [16] allows to bypass these limitations but, although also able to detect final reaction products in favourable cases, this technique is better suited for the detection of adsorbed species (usually acting as either intermediates or catalytic poisons, these two options not being mutually exclusive).

Chromatographic techniques coupled to electrochemical cells are a much better option for the detection of the final products of glycerol oxidation. By combining cyclic voltammetry with high-performance liquid chromatography (HPLC), Kwon et al. [12,17] have detected glyceric acid, glycolic acid and formic acid as the main products of the oxidation of glycerol on gold. On Pt, tartronic acid was also detected as one of the products [12,17]. More recently, Li and co-workers [6,18] have detected the production of glycerate, glycolate, tartronate, mexoxalate, oxalate and glyoxylate, with co-generation of electricity, when glycerol is oxidised at the anode of a fuel cell using gold as the anode catalyst. We find it interesting that the detection of formate was not reported, as generation of C2 products like glycolate, glyoxylate and oxalate must

necessarily result in the generation of C1 products at the same concentration. This can be considered therefore indirect evidence of complete oxidation of glycerol to carbonate.

The role of adsorbed OH (OH_{ad}) in the oxidation of glycerol on Au electrodes was recognised 36 years ago by Kahyaoglu et al. [19], who suggested that, after adsorbing on the electrode surface, glycerol reacts with OH_{ad}. In this work, we study the electro-oxidation of glycerol on polycrystalline Au in alkaline medium by combining cyclic voltammetry and potential step experiments with either ATR-SEIRAS or measurements of reflectance changes at 520 nm (this wavelength was chosen because it roughly coincides with the excitation of gold's bulk plasmon, and the reflectance is therefore very sensitive to changes in the chemical state of the electrode surface). ATR-SEIRAS allows us to detect the adsorption of reaction products, while monitoring changes in the electrode reflectance at 520 nm allows a deeper insight into the roles of OH_{ad} and gold surface oxide in the reaction, as well as into the interplay between the glycerol and surface oxidation reactions.

2. Materials and Methods

Electrolytes were prepared by dissolving KOH (≥ 85%, Sigma-Aldrich) in either ultrapure water (Milli-Q) or D_2O (99.9 atom %, Sigma-Aldrich) up to a concentration of 0.1 mol L^{-1} (approximate pH 13). Solutions containing glycerol were prepared by adding glycerol (≥ 99.5%, Sigma-Aldrich) to the desired concentration. All the experiments were performed using a flame-annealed Au wire (Alfa Aesar, 99.997% metals basis) as a counter electrode and a home-made Ag/AgCl(KCl_{sat}) electrode as reference. However, all the potentials in the text are referred to the reversible hydrogen electrode (RHE), unless otherwise stated.

All the experiments were performed under N_2 purging at room temperature. Due to the cell design, which favoured obtaining a good optical signal over efficient deoxygenation, some dissolved oxygen remained in the electrolyte during the visible reflectance experiments, as revealed, *e.g.*, by the oxygen reduction wave around 0.77 V in the cyclic voltammogram of

Fig. 1A. The working electrode for the cyclic voltammetry, current transients and reflectance experiments was a polycrystalline gold rod (Metrohm, 0.3 cm in diameter) embedded in teflon and attached to a Metrohm 628-10 rotating electrode. The rod's exposed circular face was polished with MasterPolish (Buehler, Alumina + SiO_2, 0.05 μm) and then sonicated in Ultrapure water before each experiment, immersed in the electrolyte and activated by continuous cycling between the hydrogen and oxygen evolution potential limits. The potential dependence of the electrode reflectance at 520 nm was monitored using a Teflon cell specially designed for this purpose and using a potentiostat (Metrohm Autolab, type III) to control the electrode potential and monitor the current (the cyclic voltammograms showing the effect of ohmic compensation in Fig. S1 were performed using a CHI600 potentiostat). The light from a Hg-Xe lamp (150 W) inside a Sciencetech Collimated Beam Lamp Housing was passed through a monochromator and focused on the electrode surface at normal incidence by making the beam pass through a lens and a beam splitter. The beam reflected from the electrode surface was directed to a photomultiplier tube (PMT, Hamamatsu R955) powered by a high-voltage power supply (Brandenburg, 475R). The photocurrent generated at the PMT was transformed to a voltage by a 1 kΩ resistor connected to the PMT's output and fed into the auxiliary input of the potentiostat, which allowed simultaneous recording of the potential dependence of both current and reflectance (cyclic voltammogram and reflectogram, respectively) during a potential sweep, or their time evolution after a potential step. Reflectance experiments using an RDE at 1000 rpm (Fig. 1b and Fig. 4) were very noisy due to a small precession of the RDE which we could not cancel completely. The raw data were therefore smoothed using a 15-point adjacent-averaging signal processing tool. The original unfiltered figures can be found in the Supporting Information (Figs. S2 and S3). Excluding this, no further treatment of the reflectance data was performed.

ATR-SEIRA spectra were recorded using a Nicolet iS50R FTIR spectrometer equipped with a liquid nitrogen-cooled MCT detector and a home-made ATR accessory, using unpolarized light. A new background spectrum at 0.265 V vs RHE was recorded before each spectral series. Differential spectra are reported in absorbance units, calculated as $-\log\left(\frac{R_{\text{sample}}}{R_{\text{reference}}}-\right)$, where $R_{\text{reference}}$ and R_{sample} are the reference and sample spectra, respectively. Positive bands correspond to species present in the sample spectrum that were absent in the background spectrum, while negative bands correspond to species present in the background spectrum that are absent in the sample spectrum. Series of differential spectra after a potential-step were obtained in the kinetics mode by accumulating 200 interferograms per spectrum with a spectral resolution of 4 cm^{-1}, which resulted in a time resolution of 40 s. The working electrode was an Au film deposited on the totally reflecting plane of a Si prism bevelled at 60º following a previously reported procedure [20]. The Si prism was attached to the spectroelectrochemical cell using an O-ring seal and electrical contact with the film was made by pressing onto it a circular gold wire. Before any IR measurements, the film was cycled in 0.1 mol L^{-1} H_2SO_4 then rinsed with deuterium-oxide before filling the cell with the glycerol-containing 0.1 mol L^{-1} KOH solutions in D_2O used for the experiments. Repetitive cycling in 0.1 mol L^{-1} KOH was avoided to prevent the film from peeling off the Si substrate. This also limited the potentials applied in the experiments to E < 0.9 V vs. RHE.

3. Results and discussion

Fig. 1(A) shows the cyclic voltammograms and the simultaneously recorded reflectograms (λ = 520 nm) at 0.05 V s^{-1} of a Au electrode in 0.1 mol L^{-1} KOH in the presence (red lines) and absence (black lines) of glycerol (glycerol concentration 0.3 mol L^{-1}). An excellent description of the reflection of UV-vis light by the surface of an electrode can be found in [21–23]. Detailed analysis of reflectance data requires the use of a three-layer model for which the complex dielectric constants of the electrolyte, the metal and the interface (the latter, unknown, is usually

calculated using an efficient medium model [24–27]) are required. Luckily, such a complicated treatment is often not needed, and a simple visual inspection of the reflectance data renders sufficient and valuable information [28–33].

In the absence of glycerol, an approximately linear decrease of the reflectance of the gold electrode accompanies the positive-going sweep up to approximately 1.20 V, when the reflectance decreases precipitously coinciding with the onset of gold oxide formation. A linear increase of the electrode reflectance is seen to start in the negative-going sweep just below 1.00 V, coinciding with the potential at which the gold oxide formed in the preceding positive scan has been completely reduced. This linear dependence of the surface reflectance on the potential is due to the electroreflectance of gold, a purely physical effect associated to a decrease in the density of free electrons in the metal surface with increasingly positive potential [34,35]. The electroreflectance of Au is maximum around 500 nm due to the excitation of the bulk plasmon [21]. The faster decrease in the reflectance in the positive-going sweep and the fast reflectance increase in the negative-going sweep above and below, respectively, 1.20 V, are obviously due to the formation of an oxide layer on the surface and its subsequent reduction. This signal is therefore ideal to monitor the formation of the surface oxide when the associated current is obscured by a larger one (*e.g.*, by that corresponding to the oxidation of glycerol).

Depending on the crystallographic orientation of the surface, OH adsorption on gold can occur at potentials as low as 0.15 V vs. RHE (corresponding to adsorption on Au(110) sites) and an OH adlayer on gold is completed between approximately 0.80 and 1.20 V [36]. The reflectogram in Fig. 1A shows that the reflectance of the Au surface at 520 nm is insensitive to this process.

It has been suggested that the OH adlayer facilitates the oxidation of glycerol by acting as a coupler between it and the Au surface [37]. Our results clearly show that the role of OH_{ad} goes well beyond that: OH_{ad} is the surface reactive species which successively oxidises glycerol in

a series of Langmuir-Hinshelwood steps. This is clear from the fact that the formation of the surface gold oxide layer, as detected by the sharp decrease in the surface reflectance, is delayed in the presence of glycerol (compared red and black lines in Fig. 1) and is in agreement with Kwon et al. [11], who, based on their own results and on previous DFT calculations [38] suggesting that OH_{ad} on gold lowers the barrier for β-elimination significantly, proposed that there must be some interaction between the alkoxide and the OH_{ad}-covered gold surface. This implies that (i) glycerol is oxidised by OH_{ad} in a purely chemical step, whose rate constant, k_{chem}, is therefore potential independent (please note that the rate of glycerol oxidation will still increase with potential because so does the coverage by OH_{ad}) and (ii) OH_{ad} is also the necessary precursor for the formation of a surface gold oxide layer. Initially, the reaction of adsorbed intermediates with OH_{ad} is faster than the formation of the surface oxide, which is therefore inhibited. However, as the rate constant of the oxidation of gold must increase exponentially with potential because it involves an electron transfer, the rate of this process will eventually overcome that of the reaction of OH_{ad} with adsorbed intermediates, leading to the sharp decrease in both surface reflectance and oxidation current. Increasing the concentration of glycerol or the transport rate of glycerol to the surface by, *e.g.*, using a rotating-disk electrode (RDE), expectedly leads to a larger positive shift of the potential required to form the surface oxide layer, as shown in Fig. 1B. It is evident that, by increasing the transport rate of glycerol to the surface, the onset of surface oxidation is delayed. Although a significant contribution of the uncompensated electrolyte resistance to the positive shift of the onset of surface oxidation is evident in Fig. 1B (the Metrohm Autolab type III potentiostat used in these experiments cannot correct for the *IR* drop) a separate experiment using the same glycerol concentration and the same rotation and scan rates demonstrates that the major contribution to the shift is by large that due to the increased concentration of glycerol at the

electrode-electrolyte interface when the electrode is rotated (see Fig. S1 in the Supporting Information).

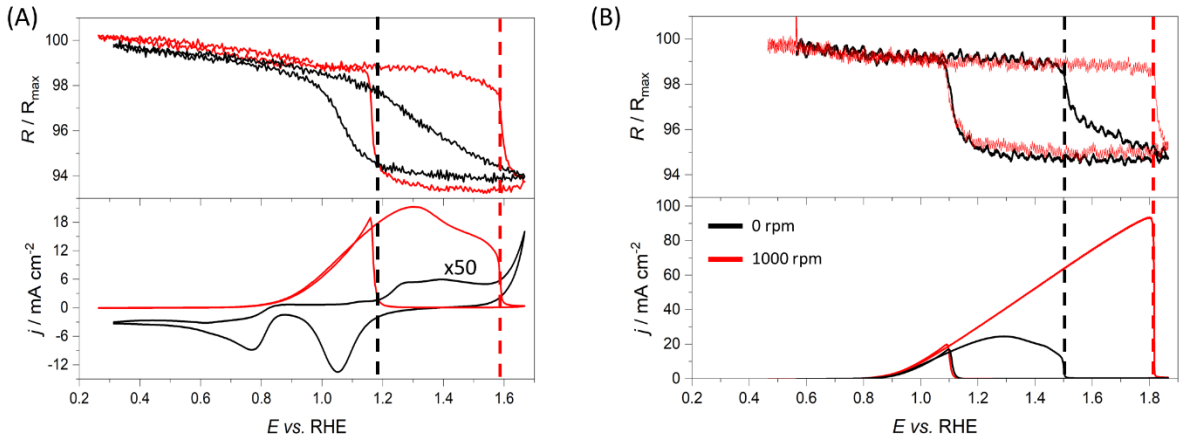

Figure 1. Reflectograms at λ = 520 nm (top panel) and cyclic voltammograms (lower panel) at 0.05 V s^{-1} of **(A)** a polycrystalline Au electrode in 0.1 mol L^{-1} KOH (black lines) and in 0.1 mol L^{-1} KOH also containing 0.3 mol L^{-1} glycerol (red lines) and **(B)** a polycrystalline Au RDE in 0.1 mol L^{-1} KOH also containing 0.05 mol L^{-1} glycerol at 0 (black lines) and 1000 rpm (red lines). The reflectogram at 1000 rpm was smoothed using an adjacent-averaging method to reduce the noise caused by the small precision of the electrode. See Fig. S2 in the Supporting Information for the unfiltered data. The dashed black and red vertical lines mark the onset of the faster decrease of the electrode reflectance due to the formation of a gold oxide layer in either the absence and presence of glycerol **(A)** or at 0 and 3000 rpm **(B)**, respectively.

While formation of OH_{ads} is necessary for the oxidation of glycerol, formation of a gold oxide layer deactivates the surface, as deduced from the perfect coincidence between the sharp decrease in the anodic current and that of the electrode reflectance in Fig. 1. Similarly, the reactivation of the surface in the negative-going sweep coincides with a very sharp increase in the electrode reflectance, *i.e.*, with the stripping of the surface oxide layer. Please note that, in the negative-going sweep, the reflectance increases faster in the presence than in the absence of glycerol, which, although slightly exaggerated by the effect of the electrolyte's uncompensated resistance, is additional evidence that both oxidation of glycerol and of the gold surface require the previous formation of OH_{ads} and compete for it.

Current transients measured after a potential step into the region just above the onset of glycerol oxidation show a relatively fast current decay over the first tens of seconds followed by a lower but continued decrease of the anodic current (Fig. 2). This current decay cannot be due to an inactivation of the electrode surface due to formation of an oxide layer, because it occurs at potentials at which formation of such layer does not occur even in the absence of glycerol (Fig. 1). There is also a slight increase of the current at $t = 0$ when the electrode is rotated at 500 rpm (Fig. 2B), as compared with a static electrode (Fig. 2A), even at the most negative potential of 0.615 V, although in this potential region the rate of the reaction must be completely controlled by kinetics and the effect of transport should be negligible (compare the currents in this potential region at 0 and 1000 rpm in Fig. 1B). This is confirmed by the fact that no further increase of the current is observed when the rotation rate is increased to 1000 rpm (Fig. 2C). The observed current decay must consequently be due to the adsorption on the surface of one or several reaction products, which accumulate at the interface as the reaction proceeds. The higher initial currents, as well as the slower initial faster current decay when the electrode is rotated, imply that transporting the products of the reaction away from the interface results in a decrease of their coverage, this is, that adsorption of these products must be reversible. This is in agreement with recent results published by Melle et al. [39] reporting galvanostatic potential oscillations during the oxidation of glycerol on Pt in acidic medium. However, they suggest that glyceraldehyde is the intermediate whose adsorption inhibits the process, while, as we will show below, our ATR-SEIRAS results suggest that one or several bridge-bonded adsorbed carboxylates are more likely candidates as the species responsible for the inhibition. Please note that the transients in Fig. 2 were measured sequentially, and therefore the concentration of the products in the bulk of the solution increased as the experiment proceeded. This explains why the initial current at 1000 rpm is slightly lower than at 500 rpm.

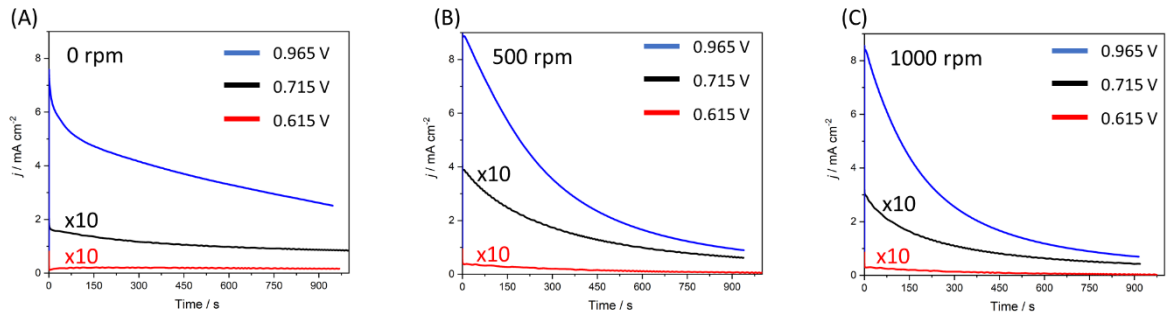

Figure 2. Current transients recorded with a polycrystalline Au RDE in 0.1 mol L^{-1} KOH containing 0.1 mol L^{-1} glycerol after a potential step from 0.265 V vs. RHE to 0.615 (red lines), 0.715 (black lines) and 0.965 (blue lines) V at 0 (A), 500 (B) and 1000 (C) rpm.

Although very sensitive to the formation of an oxide layer on the electrode surface, visible reflectance measurements at normal incidence are not sensitive to adsorbed intermediates or products formed during the reaction, for which ATR-SEIRAS is much better suited. As carboxylates are the main (if not the only) expected products of glycerol oxidation [7,8,14,15,40], ATR-SEIRAS monitoring of species at the interface after a potential step was done using D_2O as solvent, to avoid masking of the asymmetric stretching of carboxylates by the $\delta_{H\text{-}O\text{-}H}$, band of H_2O.

Fig. 3(B) shows ATR-SEIRA spectra of a Au film electrode deposited on Si in 0.1 mol L^{-1} KOH (D_2O) containing 0.5 mol L^{-1} glycerol, collected at 40 s intervals after a potential step from 0.265 V to 0.465, 0.565, 0.665, 0.765 and 0.865 V. A spectrum collected at 0.265 V before each potential step was used as background. The simultaneously recorded current transients are shown in Fig. 3(A).

At 0.465 V, before any measurable anodic current can be detected, only small bands around 1431 and 1330 cm^{-1} can be seen. This bands are present in the ATR spectrum of glycerol (see Supporting Information, Fig. S4), and correspond to glycerol's CH_2 and CH stretching, CH_2-bending and C-H bending modes, respectively [41,42]. This suggests the adsorption of glycerol

after a positive potential step, which is in agreement with the fact that, as discussed above, deprotonated glycerol must be the reacting species. Assignment of these bands to adsorbed deprotonated glycerol is supported by their absence at more positive potentials, beyond the onset of glycerol oxidation, where the reaction should result in a decreased coverage by this species. Please note that the experiments in Fig. 3 were done in the potential region where the reaction rate is controlled by the kinetics of the reaction, and the concentration of glycerol will remain equal or very close to that in the bulk. In good agreement with this, no negative bands suggesting a decrease in the concentration of glycerol at the interface can be observed in the spectra.

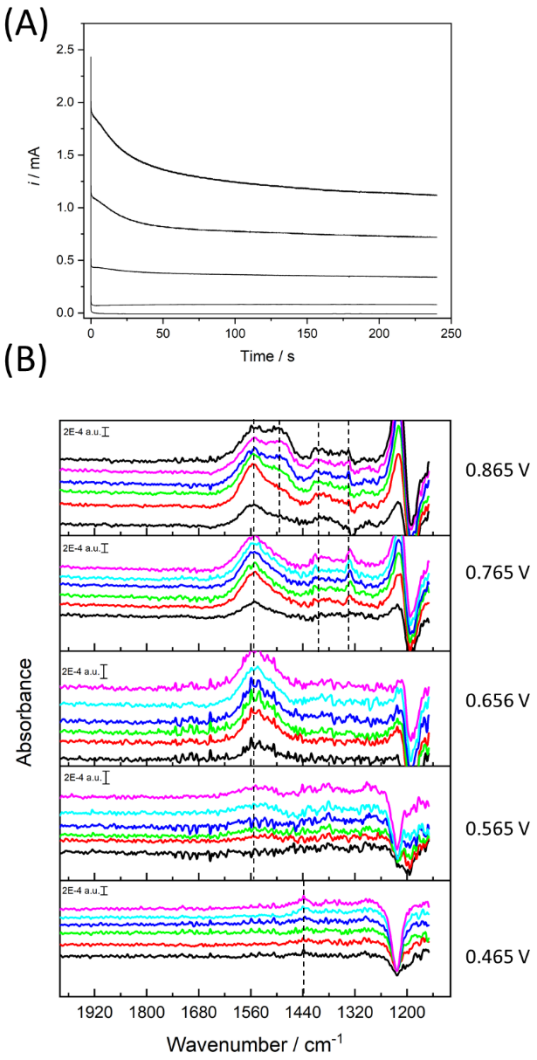

Figure 3. ATR-SEIRA spectra of the Au-electrolyte interface in 0.1 mol L^{-1} KOH containing 0.5 mol L^{-1} glycerol in D_2O, collected during the first 250 s after a potential step from 0.265 V vs. RHE to 0.465, 0.565, 0.665, 0.765 and 0.865 V (B). Spectral resolution is 4 cm^{-1}. Each spectrum consists of 200 interferograms, which resulted in a time interval between spectra of 40 s, which allowed for sufficient accumulation of reaction products. The simultaneously measured current transients are shown in (A). The reference spectrum was taken at 0.265 V.

The bands described above are also visible at 0.565 V, but a new band around 1540 cm^{-1}, right in the middle of the spectral region characteristic for the anti-symmetric stretching mode of carboxylate groups [8,15,43], appears at this potential, the intensity of which increases during the first 80 s at all the potentials. At 0.765 V it becomes evident that this band is accompanied by two weaker bands around 1400 cm^{-1} and at 1332 cm^{-1}, and a two-dimensional analysis of the spectra at this potential (see Supporting Information, Fig. S5) confirms that these three bands grow synchronously. They must therefore correspond to either the same species or to

two species in equilibrium with each other. The carboxylate responsible for the antisymmetric O-C-O stretching band around 1540 cm^{-1} cannot be directly adsorbed on the electrode surface, as this mode is prohibited by the surface selection rule [16]. This band must therefore correspond either to a carboxylate in the solution or to the carboxylate group facing the solution of an adsorbed C3 dicarboxylate (note that the dynamic dipole moment of the asymmetric O-C-O stretching of the carboxylate group facing the solution of the only possible C2 carboxylate, oxalate, would be parallel to the electrode surface, and would therefore also be prohibited by the surface selection rule of ATR-SEIRAS). We attribute the band around 1400 cm^{-1} to the corresponding symmetric carboxylate stretching. The band at 1332 cm^{-1} must correspond to the symmetric stretching of a bidentate adsorbed carboxylate [44–47]. In all the spectra shown, the intensity of these three bands increases between the first and the second spectra (accumulated during the first 40 s and between 40 and 80 s after the potential step), and remains roughly constant afterwards, which is consistent with the simultaneously recorded current transients, in which the largest current decay occurs during the first 50 s after the potential step.

In acidic media, adsorbed bidentate formate, acetate, oxalate, malonate and succinate adsorbed on Au appear around 1330 cm^{-1},[44] 1400 cm^{-1},[45] 1300 cm^{-1},[46] 1380 cm^{-1} [47] and 1390 cm^{-1} [47], respectively. At first sight, adsorbed bidentate formate might appear the most likely candidate for the band observed at 1332 cm^{-1}. However, it must be recalled that the frequency of adsorbed species typically decreases with increasingly negative potential and that, in a pH-independent reference scale, the potential window in alkaline solutions is considerably more negative than that in acidic solutions. Consequently, any of the other carboxylates detected in previous work using HPLC, like, *e.g.*, glycoxylate or glycerate, may also be responsible for this band. In any case, it is not the aim of this work to identify the products of the reaction, for which other techniques like HPLC are better suited than ATR-SEIRAS and which has been reported before. Our goal is rather to show that the carboxylates produced do adsorb on the

surface and are responsible for inhibiting the reaction, and the results reported in Fig. 3 provide strong evidence for this.

At 0.865 V, the band around 1330 cm^{-1} is negative, suggesting the corresponding carboxylate product was already adsorbed at the background potential (0.265 V) and has partially desorbed at 0.865 V. Please note that the spectral series in Fig. 3 were recorded sequentially and a non-negligible concentration of reaction products must already be present in the solution by the time the series at 0.865 V was started. Therefore, the presence of an adsorbed bidentate carboxylate on the surface at 0.265 V, despite no reaction happening at this potential, is not surprising. Its desorption at 0.865 V suggests that OH^- and the carboxylate product(s) compete for the adsorption sites on the surface, as would be expected because both are specifically adsorbing anions.

A second band appears at 0.865 V in the spectral region characteristic for the symmetric stretching of carboxylates. This is consistent with the multiplicity of carboxylates detected as reaction products in previous work using HPLC [6,12,17,18]. There is also an increased absorption intensity in the region between 1300 and 1450 cm^{-1}, which could be due to additional carboxylate symmetric stretching bands (both bidentate adsorbed and in solution or adsorbed but facing the solution). However, they are too week for a deeper analysis. No evidence of formation of carbonate due to the complete oxidation of glycerol can be found in the spectra within the potential region explored, although the carbonate band could well be buried within the intensity in the region around 1400 cm^{-1}.

The competition between the caboxylate products and OH^- for the adsorption sites on the electrode surface implies that the inhibiting effect of the adsorbed carboxylate(s) is double, as it will prevent the adsorption on the surface of the two reactive species needed, namely, deprotonated glycerol and OH_{ad}. A third effect occurs at potentials positive enough to oxidise

the surface. Under these conditions, adsorption of the reaction products will decrease the rate at which OH_{ad} is removed by reacting with glycerol, eventually leading to the oxidation of the surface happening faster than that of glycerol, to the formation of an oxide layer and, consequently, to a complete inhibition of the reaction. Such behaviour is illustrated in Fig. 4, showing potentiostatic reflectance transients at l = 520 nm of a Au RDE in glycerol-containing 0.1 mol L^{-1} KOH alongside simultaneously recorded current transients after a potential step to 1.415 V (well into the oxide region) at different rotation rates. The first interesting observation in Fig.4 is that the initial current is the same in all the transients, suggesting that, at this very positive potential, at which a complete OH adlayer must form instantaneously, the rate of the reaction is determined by the sites available on the surface for the adsorption of deprotonated glycerol. This confirms our statement above that the oxidation of glycerol happens via one or several Langmuir-Hinshelwood steps involving, on one side, deprotonated glycerol and other reaction intermediates and, on the other, OH_{ad}.

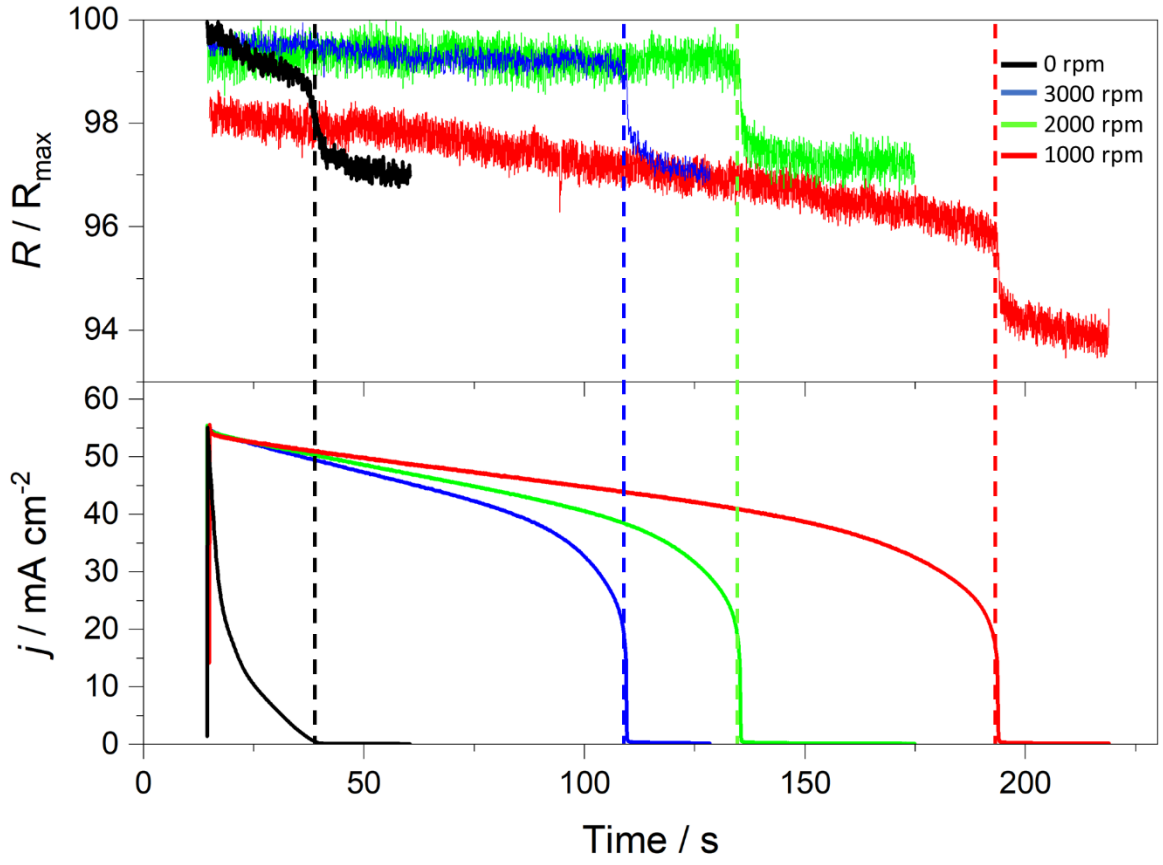

Figure 4. Potentiostatic reflectance (top) and current (bottom) transients recorded with a Au RDE in 0.1 mol L^{-1} KOH containing 0.05 mol L^{-1} glycerol after a potential step from 0.265 to 1.415 V vs. RHE. λ = 520 nm. Rotation rate: 0 (black), 1000 (red), 2000 (green) and 3000 (blue) rpm. The reflectogram at 1000 rpm was smoothed using an adjacent-averaging method to reduce the noise caused by the small precision of the electrode. See Fig. S3 in the Supporting Information for the unfiltered data.

All the current transients in Fig. 4 show a sudden and nearly complete deactivation of the surface after a time which depends on the rotation rate. The concomitant decrease of the electrode reflectance is clear evidence that this deactivation is due to a sudden oxidation of the surface. However, this is only possible if the rate of oxidation of glycerol has previously decreased to a point at which further oxidation of OH_{ad} to gold oxide is faster than its removal by glycerol. This decrease of the reaction rate has to be due to the adsorption of the carboxylate products of the reaction because (i) its accompanied by a negligible (1000, 2000 and 3000 rpm)

or comparatively small (0 rpm) decrease of the surface reflectance and (ii) the decay of the reaction rate is very fast when the transport of products away from the electrode surface is accelerated by rotating the electrode, which also results in a delay of the complete deactivation of the surface to longer times. Somehow counterintuitively, the reflection and current transients at the two highest rotation rates of 2000 and 3000 rpm show that the oxidation and consequent deactivation of the electrode surface occur at shorter times than with a rotation rate of 1000 rpm. As in the experiments above, these transients were measured sequentially, which resulted in a gradual accumulation of reaction products in the solution. As a consequence, at the two higher rotation rates the concentration of reaction products at the interface must be higher than at 1000 rpm. Actually, this result is additional evidence that the carboxylates produced upon oxidation of glycerol adsorb reversibly on the surface. To prove our point, potential steps at the same rotating rates but using a fresh solution and a pristine gold electrode for each rotating rate are shown in the Supporting Information (Fig. S6). Under these conditions, higher rotating rates lead to longer times needed for the formation of gold oxide.

4. Conclusions

By combining cyclic voltammetry and potentiostatic current transients with in situ ATR-SEIRAS and visible reflectance measurements, we have obtained important insight into the electrocatalytic oxidation of glycerol on gold electrodes.

Our results show that the oxidation of glycerol involves one or (most likely) several Langmuir-Hinshelwood steps in which adsorbed deprotonated glycerol and other intermediates react with OH_{ad}. However, further oxidation of the surface to form an oxide layer results in a complete deactivation for the oxidation of glycerol. Glycerol oxidation and the formation of a surface oxide layer compete for OH_{ad}, which retards the oxidation of the gold surface in the presence of glycerol. A similar conclusion was reached for several alcohols and platinum by Santiago et

al. [48], suggesting that this reaction mechanism might be general for all metals and all alcohols, with the exception of methanol at least in the case of Pt [48].

We have also shown that the carboxylates resulting from the oxidation of glycerol adsorb on the surface and have an inhibiting effect on the reaction rate. However, this is not a major drawback, as the adsorption is reversible and the surface coverage by adsorbed products can be decreased (thereby maintaining a high activity) if they are transported away from the interface.

Our results are relevant for the design of fuel cells capable of generating electricity plus value-added chemicals (carboxylic acids resulting from the oxidation of glycerol). As the reaction requires OH_{ad}, materials on whose surface this species can be formed as negative as possible should be used. However, care must be taken because these materials will also form an oxide layer at relatively negative potentials which, as we have demonstrated here, may result in the deactivation of the surface. The flow rate of the fuel feed into the cell must also be carefully designed to maintain a low concentration of products at the interface while at the same time allowing for a high conversion of the reactant.

Acknowledgements

The support of the Leverhulme Trust through the Doctoral Scholarship Scheme [DS-2017-073] is gratefully acknowleged.

REFERENCES

[1] G. Dodekatos, S. Schünemann, H. Tüysüz, Recent Advances in Thermo-, Photo-, and Electrocatalytic Glycerol Oxidation, ACS Catal. 8 (2018) 6301–6333. https://doi.org/10.1021/acscatal.8b01317.

[2] A. Demirbas, Political, economic and environmental impacts of biofuels: A review, Appl. Energy 86 (2009) S108–S117. https://doi.org/10.1016/j.apenergy.2009.04.036.

[3] P. Parpot, A.P. Bettencourt, G. Chamoulaud, K.B. Kokoh, E.M. Belgsir,

Electrochemical investigations of the oxidation-reduction of furfural in aqueous medium - Application to electrosynthesis, Electrochim. Acta 49 (2004) 397–403. https://doi.org/10.1016/j.electacta.2003.08.021.

[4] T. Łuczak, M. Bełtowska-Brzezinska, R. Holze, Molecular structure effects in the adsorption of terminal and vicinal aliphatic diols on a gold electrode, Electrochim. Acta 38 (1993) 717–720. https://doi.org/10.1016/0013-4686(93)80243-S.

[5] C.L. D. Takky, B. Beden, J.M. Leger, Evidence for the effect of molecular structure on the electrochemical reactivity of alcohols: Part I. Electrooxidation of the butanol somers on noble metal electrodes in alkaline medium, J. Electroanal. Chem. 145 (1923) 461–466. https://doi.org/10.1016/S0022-0728(83)80101-6.

[6] J. Qi, L. Xin, D.J. Chadderdon, Y. Qiu, Y. Jiang, N. Benipal, C. Liang, W. Li, Electrocatalytic selective oxidation of glycerol to tartronate on Au/C anode catalysts in anion exchange membrane fuel cells with electricity cogeneration, Appl. Catal. B 154–155 (2014) 360–368. https://doi.org/10.1016/j.apcatb.2014.02.040.

[7] M. Simões, S. Baranton, C. Coutanceau, Electro-oxidation of glycerol at Pd based nano-catalysts for an application in alkaline fuel cells for chemicals and energy cogeneration, Appl. Catal. B 93 (2010) 354–362. https://doi.org/10.1016/j.apcatb.2009.10.008.

[8] M. Simões, S. Baranton, C. Coutanceau, Electrochemical valorisation of glycerol, ChemSusChem 5 (2012) 2106–2124. https://doi.org/10.1002/cssc.201200335.

[9] H. Habe, T. Fukuoka, D. Kitamoto, K. Sakaki, Biotechnological production of d-glyceric acid and its application, Appl. Microbiol. Biotechnol. 84 (2009) 445–452. https://doi.org/10.1007/s00253-009-2124-3.

[10] A. Ilie, M. Simoes, S. Baranton, C. Coutanceau, S. Martemianov, Influence of operational parameters and of catalytic materials on electrical performance of Direct

Glycerol Solid Alkaline Membrane Fuel Cells, J. Power Sources 196 (2011) 4965–4971. https://doi.org/10.1016/j.jpowsour.2011.02.003.

[11] Y. Kwon, S.C.S. Lai, P. Rodriguez, M.T.M. Koper, Electrocatalytic oxidation of alcohols on gold in alkaline media: Base or gold catalysis?, J. Am. Chem. Soc. 133 (2011) 6914–6917. https://doi.org/10.1021/ja200976j.

[12] Y. Kwon, K.J.P. Schouten, M.T.M. Koper, Mechanism of the Catalytic Oxidation of Glycerol on Polycrystalline Gold and Platinum Electrodes, ChemCatChem 3 (2011) 1176–1185. https://doi.org/10.1002/cctc.201100023.

[13] M.B.C. De Souza, V.Y. Yukuhiro, R.A. Vicente, C.T.G. Vilela Menegaz Teixeira Pires, J.L. Bott-Neto, P.S. Fernández, Pb- And Bi-Modified Pt Electrodes toward Glycerol Electrooxidation in Alkaline Media. Activity, Selectivity, and the Importance of the Pt Atoms Arrangement, ACS Catal. 10 (2020) 2131–2137. https://doi.org/10.1021/acscatal.9b04805.

[14] J.F. Gomes, G. Tremiliosi-Filho, Spectroscopic Studies of the Glycerol Electro-Oxidation on Polycrystalline Au and Pt Surfaces in Acidic and Alkaline Media, Electrocatalysis 2 (2011) 96–105. https://doi.org/10.1007/s12678-011-0039-0.

[15] D.Z. Jeffery, G.A. Camara, The formation of carbon dioxide during glycerol electrooxidation in alkaline media: First spectroscopic evidences, Electrochem. Commun. 12 (2010) 1129–1132. https://doi.org/10.1016/j.elecom.2010.06.001.

[16] R. Kas, O. Ayemoba, N.J. Firet, J. Middelkoop, W.A. Smith, A. Cuesta, In-Situ Infrared Spectroscopy Applied to the Study of the Electrocatalytic Reduction of CO_2: Theory, Practice and Challenges, ChemPhysChem 20 (2019) 2904–2925. https://doi.org/10.1002/cphc.201900533.

[17] Y. Kwon, M.T.M. Koper, Combining voltammetry with HPLC: Application to electro-oxidation of glycerol, Anal. Chem. 82 (2010) 5420–5424.

https://doi.org/10.1021/ac101058t.

[18] L. Xin, Z. Zhang, Z. Wang, W. Li, Simultaneous Generation of Mesoxalic Acid and Electricity from Glycerol on a Gold Anode Catalyst in Anion-Exchange Membrane Fuel Cells, ChemCatChem 4 (2012) 1105–1114. https://doi.org/10.1002/cctc.201200017.

[19] C.L. A. Kahyaoglu, B. Beden, Oxydation electrocatalitique du glycerol sur electrodes d'or et de platine en milieu aqueux, Electrochim. Acta 29 (1984) 1489–1492. https://doi.org/10.1016/0013-4686(84)87033-4.

[20] T.Y. Masatoshi Osawa, Ken-ichi Ataka, Katsumasa Yoshii, Surface-enhanced infrared ATR spectroscopy for in situ studies of electrode/electrolyte interfaces, J. Electron Spectrosc. Relat. Phenom. 64–65 (1993) 371–379. https://doi.org/10.1016/0368-2048(93)80099-8.

[21] D.M. Kolb, UV-Visible Reflectance Spectroscopy, in: Spectroelectrochemistry, Gale R.J. (Ed.), Springer, Boston, 1988: pp. 87–188. https://doi.org/10.1007/978-1-4613-0985-7_4.

[22] D. Kolb, SPECTROSCOPIE ET RÉFLECTANCEREFLECTANCE SPECTROSCOPY IN THE STUDY OF ELECTRODE SURFACES, J. Phys. Colloq. 38 (1977) C5-167-C5-177.

[23] D.M. Kolb, Electroreflectance Spectroscopy in the Study of Metal-Electrolyte Interfaces., J. Phys. Colloq. 44 (1983) C10-137–C10-146. https://doi.org/10.1051/jphyscol:19831029.

[24] D.A.G. Bruggeman, Berechnung verschiedener physikalischer Konstanten von heterogenen Substanzen. III. Die elastischen Konstanten der quasiisotropen Mischkörper aus isotropen Substanzen, Ann. Phys. 421 (1937) 160–178. https://doi.org/10.1002/andp.19374210205.

[25] R. Landauer, The Electrical Resistance of Binary Metallic Mixtures, J. Appl. Phys. 23 (1952) 779–784. https://doi.org/10.1063/1.1702301.

[26] C. Pecharromán, J.E. Iglesias, Effective dielectric properties of packed mixtures of insulator particles, Phys. Rev. B 49 (1994) 7137–7147. https://doi.org/10.1103/PhysRevB.49.7137.

[27] C. Pecharromán, A. Cuesta, C. Gutiérrez, Calculation of adsorption-induced differential external reflectance infrared spectra of particulate metals deposited on a substrate, J. Electroanal. Chem. 563 (2004) 91–109. https://doi.org/10.1016/j.jelechem.2003.09.013.

[28] A. Cuesta, C. Gutiérrez, Confirmation by differential reflectance spectroscopy of the transition at 270 nm of CO chemisorbed on Pt in an acid medium, J. Electroanal. Chem. 383 (1995) 195–197. https://doi.org/10.1016/0022-0728(94)03760-Z.

[29] M. Sistiaga, A. Cuesta, A.R. Pierna, C. Gutiérrez, Characterization by electrolyte electroreflectance and X-ray photoelectron spectroscopy of amorphous $Ni_{59}Nb_{40}Pt_{1-x}Sn_x$ alloys and their activation by HF solutions, Surf. Sci. 410 (1998) 312–320. https://doi.org/10.1016/S0039-6028(98)00330-6.

[30] A. Cuesta, N. López, C. Gutiérrez, Electrolyte electroreflectance study of carbon monoxide adsorption on polycrystalline silver and gold electrodes, Electrochim. Acta 48 (2003) 2949–2956. https://doi.org/10.1016/S0013-4686(03)00360-8.

[31] R. Díaz, S. Joiret, Á. Cuesta, I. Díez-Pérez, P. Allongue, C. Gutiérrez, P. Gorostiza, F. Sanz, Electrochemically grown tin oxide thin films: In situ characterization of electronic properties and growth mechanism, J. Phys. Chem. B 108 (2004) 8173–8181. https://doi.org/10.1021/jp037530c.

[32] Á. Cuesta, C. Borrás, Detection of surface chirality by electrolyte electroreflectance rotational anisotropy, J. Phys. Chem. C 111 (2007) 14290–14292.

https://doi.org/10.1021/jp075895h.

[33] F.W. Hartl, H. Varela, A. Cuesta, The oscillatory electro-oxidation of formic acid: Insights on the adsorbates involved from time-resolved ATR-SEIRAS and UV reflectance experiments, J. Electroanal. Chem. 840 (2019) 249–254. https://doi.org/10.1016/j.jelechem.2019.04.015.

[34] T. Takamura, K. Takamura, W. Nippe, E. Yeager, Specular Reflection Studies of Gold Electrodes in situ, J. Electrochem. Soc. 117 (1970) 626-630. https://doi.org/10.1149/1.2407591.

[35] Y. V. Tolmachev, D.A. Scherson, The electrochemical oxidation of sulfite on gold: UV-Vis reflectance spectroscopy at a rotating disk electrode, Electrochim. Acta 49 (2004) 1315–1319. https://doi.org/10.1016/j.electacta.2003.07.018.

[36] D.W. Kirk, The Electrochemical Formation of Au(I) Hydroxide on Gold in Aqueous Potassium Hydroxide, J. Electrochem. Soc. 127 (1980) 1069-1076. https://doi.org/10.1149/1.2129819.

[37] X. Shi, D.E. Simpson, D. Roy, The role of chemisorbed hydroxyl species in alkaline electrocatalysis of glycerol on gold, Phys. Chem. Chem. Phys. 17 (2015) 11432–11444. https://doi.org/10.1039/c5cp00313j.

[38] B.N. Zope, D.D. Hibbitts, M. Neurock, R.J. Davis, Reactivity of the Gold/Water Interface During Selective Oxidation Catalysis, Science 330 (2010) 74-78. https://doi.org/10.1126/science.1195055.

[39] G.B. Melle, E.G. Machado, L.H. Mascaro, E. Sitta, Eff ect of mass transport on the glycerol electro-oxidation, Electrochim. Acta 296 (2019) 972–979. https://doi.org/10.1016/j.electacta.2018.11.085.

[40] C. Coutanceau, S. Baranton, R.S.B. Kouamé, Selective Electrooxidation of Glycerol Into Value-Added Chemicals: A Short Overview, Front. Chem. 7 (2019) 1–15.

https://doi.org/10.3389/fchem.2019.00100.

[41] M. Danish, M.W. Mumtaz, M. Fakhar, U. Rashid, Response surface methodology based optimized purification of the residual glycerol from biodiesel production process, Chiang Mai J. Sci. 44 (2017) 1570–1582.

[42] J.R. Copeland, G.S. Foo, L.A. Harrison, C. Sievers, In situ ATR-IR study on aqueous phase reforming reactions of glycerol over a Pt/γ-Al_2O_3 catalyst, Catal. Today 205 (2013) 49–59. https://doi.org/10.1016/j.cattod.2012.08.002.

[43] J. Schnaidt, M. Heinen, D. Denot, Z. Jusys, R. Jürgen Behm, Electrooxidation of glycerol studied by combined in situ IR spectroscopy and online mass spectrometry under continuous flow conditions, J. Electroanal. Chem. 661 (2011) 250–264. https://doi.org/10.1016/j.jelechem.2011.08.011.

[44] A. Cuesta, G. Cabello, F.W. Hartl, M. Escudero-Escribano, C. Vaz-Domínguez, L.A. Kibler, M. Osawa, C. Gutiérrez, Electrooxidation of formic acid on gold: An ATR-SEIRAS study of the role of adsorbed formate, Catal. Today 202 (2013) 79–86. https://doi.org/10.1016/j.cattod.2012.04.022.

[45] A. Berná, J.M. Delgado, J.M. Orts, A. Rodes, J.M. Feliu, Spectroelectrochemical study of the adsorption of acetate anions at gold single crystal and thin-film electrodes, Electrochim. Acta 53 (2008) 2309–2321. https://doi.org/10.1016/j.electacta.2007.09.055.

[46] A. Berná, J.M. Delgado, J.M. Orts, A. Rodes, J.M. Feliu, In-situ infrared study of the adsorption and oxidation of oxalic acid at single-crystal and thin-film gold electrodes: A combined external reflection infrared and ATR-SEIRAS approach, Langmuir 22 (2006) 7192–7202. https://doi.org/10.1021/la060400l.

[47] J.M. Delgado, A. Berná, J.M. Orts, A. Rodes, J.M. Feliu, In Situ infrared study of the adsorption and surface acid-base properties of the anions of dicarboxylic acids at gold

single crystal and thin-film electrodes, J. Phys. Chem. C 111 (2007) 9943–9952. https://doi.org/10.1021/jp071489m.

[48] P.V.B. Santiago, R.A.G. Oliveira, J.M. Roquetto, N. Akiba, I. Gaubeur, C.A. Angelucci, J. Souza-Garcia, J.M. Feliu, Oxide formation as probe to investigate the competition between water and alcohol molecules for OH species adsorbed on platinum, Electrochim. Acta 317 (2019) 694–700. https://doi.org/10.1016/j.electacta.2019.06.037.

Reactive and inhibiting species in the electrocatalytic oxidation of glycerol on gold. A study combining in-situ visible reflectance and ATR-SEIRAS

Laura Pérez-Martínez, Lisa Balke and Angel Cuesta*.

School of Natural and Computing Sciences, University of Aberdeen, Aberdeen AB24 3UE, Scotland, UK

*Corresponding author: angel.cuestaciscar@abdn.ac.uk

SUPPLEMENTARY FIGURES

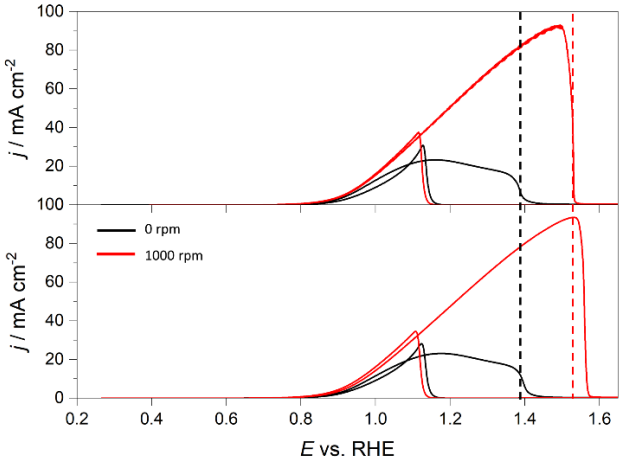

Figure S1. Cyclic voltammograms at 0.05 Vs^{-1} of a polycrystalline Au RDE in 0.1 M KOH also containg 0.05 mol L^{-1} glycerol at 0 (black lines) and 1000 rpm (red lines). The botom panel corresponds to experiments without ohmic compensation, while the cyclic voltammograms in the top panel have been corrected for the electrolyte resistance (R_u = 6.3 Ω).

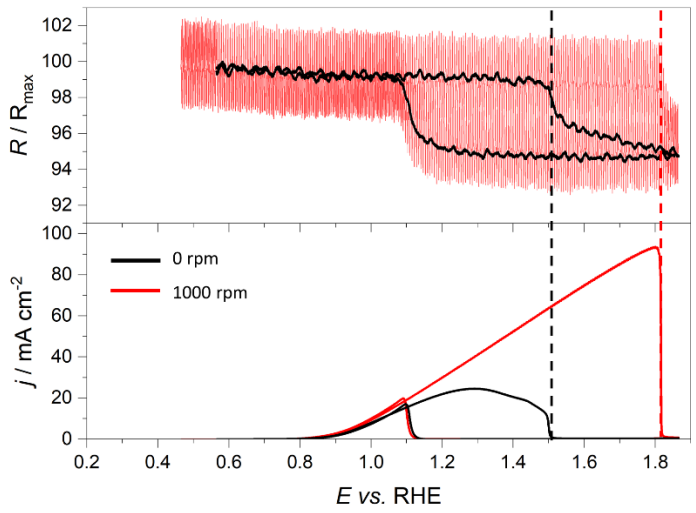

Figure S2. Unfiltered reflectograms at λ = 520 nm (top panel) and cyclic voltammograms (lower panel) at 0.05 V s^{-1} of (A) a polycrystalline Au electrode in 0.1 mol L^{-1} KOH (black lines) and in 0.1 mol L^{-1} KOH also containing 0.3 mol L^{-1} glycerol (red lines) and (B) a polycrystalline Au RDE in 0.1 mol L^{-1} KOH also containing 0.05 mol L^{-1} glycerol at 0 (black lines) and 1000 rpm (red lines). The dashed black and red vertical lines mark the onset of the faster decrease of the electrode reflectance due to the formation of a gold oxide layer in either the absence and presence of glycerol (A) or at 0 and 3000 rpm (B), respectively.

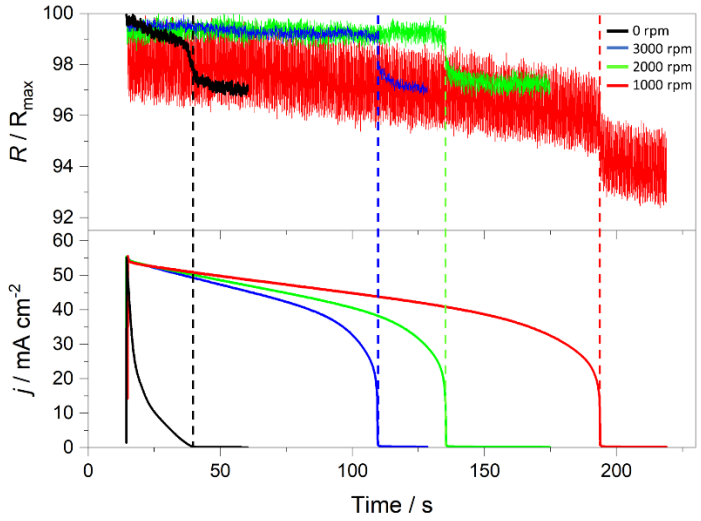

Figure S3. Original unfiltered: Potentiostatic reflectance (top) and current (bottom) transients recorded with a Au RDE in 0.1 mol L^{-1} KOH containing 0.05 mol L^{-1} glycerol after apotential stpe from 0.265 to 1.415 V vs. RHE. λ = 520 nm. Rotation rate: 0 (black), 1000 (red), 2000 (green) and 3000 (blue) rpm.

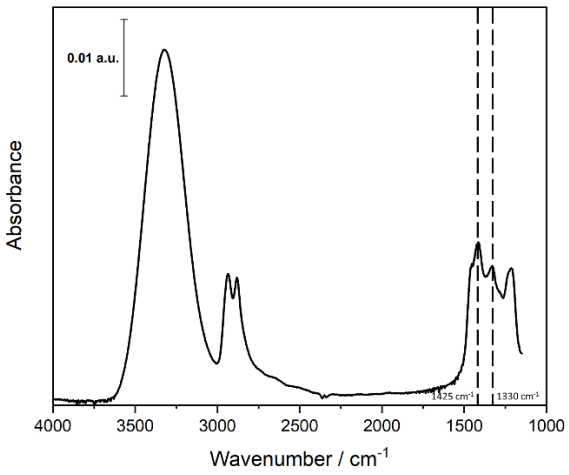

Figure S4. Transmission spectrum recorded in the ATR mode of pure glycerol on a silicon prism. The reference spectrum was the bare silicon prism.

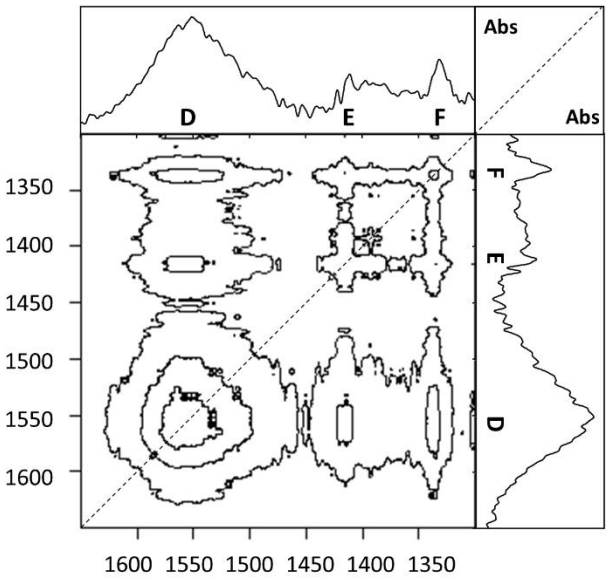

Figure S5. Synchronous 2D IR correlation plots from a series of ATR-SEIRA spectra recorded at 0.765 V during 250 in 0.1 M KOH + 0.5 M glycerol. Cross peaks connecting two bands at different frequencies imply that these two bands grow synchronously. Calculated with 2Dshige version 1.3 program [1] with permission.

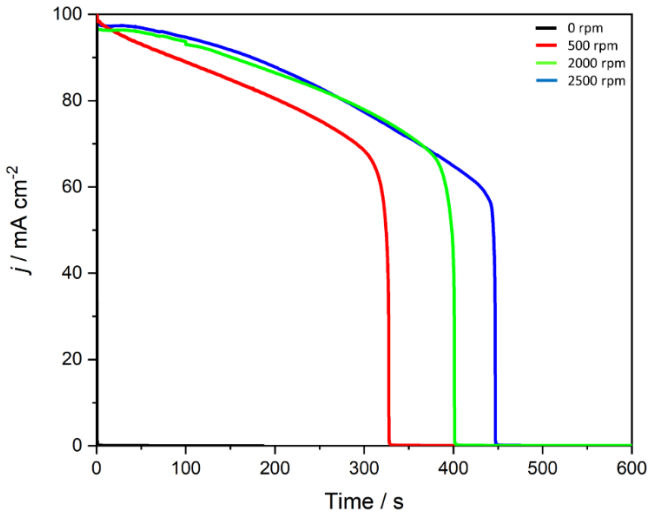

Figure S6. Current transients recorded with a Au RDE in 0.1 mol L^{-1} KOH containing 0.1 mol L^{-1} glycerol after a potential step from 0.265 to 1.515 V vs. RHE. Rotation rate: 0 (black), 500 (red), 2000 (green) and 2500 (blue) rpm. Fresh solutions and npristine working electrodes were used in each experiment.

REFERENCES

[1] 2Dshige (c) Shigeaki Morita, Kwansei-Gakuin University (2004-2005) <http://sci-tech.ksc.kwansei.ac.jp/~ozaki/>.